Research Square

Preprints are preliminary reports that have not undergone peer review.
They should not be considered conclusive, used to inform clinical practice,
or referenced by the media as validated information.

An Interpretable Model for Predicting Occult Lymph Node Metastasis in Clinical T1N0 Non-Small Cell Lung Cancer with a Consolidation-to-Tumour Ratio > 0.5: A Multicentre Study

Yanmin Zhou
Affiliated Hospital of Southwest Medical University
Dengguo Zhang
Affiliated Hospital of Southwest Medical University
Zhengpan Wei
First Affiliated Hospital of Zhengzhou University
Jiangtao Pu
Affiliated Hospital of Southwest Medical University
Biao Wang
Affiliated Hospital of Southwest Medical University
Xiangnan Li
First Affiliated Hospital of Zhengzhou University
Zhulin Wang
drwangzhulin2020@163.com

Affiliated Hospital of Southwest Medical University

Research Article

Keywords: Non-small cell lung cancer, Occult lymph node metastasis, Machine learning, Consolidation-to-tumor ratio, Explainable artificial intelligence.

Posted Date: November 12th, 2026

DOI: https://doi.org/10.21203/rs.3.rs-11458105/v1

License: This work is licensed under a Creative Commons Attribution 4.0 International License.
Read Full License

Additional Declarations: No competing interests reported.

An Interpretable Model for Predicting Occult Lymph Node Metastasis in Clinical T1N0 Non-Small Cell Lung Cancer with a Consolidation-to-Tumour Ratio > 0.5: A Multicentre Study

Yanmin Zhou[1†], Dengguo Zhang[2†], Zhengpan Wei[3], Jiangtao Pu[2], Biao Wang[2], Xiangnan Li[3*], Zhulin Wang[2*]

1 Department of Surgery, Affiliated Hospital of Southwest Medical University, Luzhou 646000, Sichuan Province, China

2 Department of Thoracic Surgery, Affiliated Hospital of Southwest Medical University, Luzhou 646000, Sichuan Province, China

3 Department of Thoracic Surgery, First Affiliated Hospital of Zhengzhou University, Zhengzhou 450052, Henan Province, China

†These authors contributed equally to this work and share first authorship.

*Corresponding authors:

Correspondence should be addressed to Zhulin Wang (drwangzhulin2020@163.com) and Xiangnan Li (lxn-2000@163.com).

Abstract

Background: Occult lymph node metastasis (oLNM) remains a concern in clinical T1N0 non-small cell lung cancer (NSCLC). In this study, we developed and externally validated a preoperative prediction model for patients with a consolidation-to-tumour ratio (CTR) of >0.5.

Methods: This retrospective study included 1,784 patients from the development

centre and 525 from an independent external validation centre. All patients had clinical T1N0 NSCLC, a tumour diameter ≤3 cm, and a CTR > 0.5, and they all underwent pulmonary resection with systematic lymph node dissection. We compared 12 machine-learning algorithms using 46 candidate preoperative features and assessed their discrimination, calibration, and potential clinical utility. SHapley Additive exPlanations (SHAP) was used to quantify feature contributions. An exploratory analysis was conducted to examine patients with tumours >2 to ≤3 cm.

Results: oLNM was detected in 295 patients (16.5%) in the development cohort and 97 (18.5%) in the external cohort. The final 10-feature CatBoost model had an area under the receiver operating characteristic curve (AUC) of 0.870 (95% CI, 0.827–0.906) in the internal validation cohort and 0.855 (95% CI, 0.814–0.895) in the external validation cohort. Among 296 patients with tumours >2 to ≤3 cm in the external validation cohort, 68 had oLNM; the AUC was 0.852 (95% CI, 0.802–0.898). External calibration revealed some risk overestimation at intermediate-to-high predicted probabilities. SHAP was applied to determine feature contributions across the cohort and for individual patients.

Conclusions: The model showed good discrimination of preoperative oLNM risk assessment in this population. Prospective validation of the developed model is required before its predictions can be used to guide the extent of nodal assessment or dissection.

Keywords

Non-small cell lung cancer; Occult lymph node metastasis; Machine learning;

Consolidation-to-tumor ratio; Explainable artificial intelligence.

Background

Patients with clinically node-negative (cN0) non-small cell lung cancer (NSCLC) can develop regional nodal metastasis, which is detected only on pathological examination after resection [1, 2]. Nodal involvement changes the pathological stage and informs postoperative treatment [3]. Preoperative imaging and, when indicated, invasive staging reduce uncertainty but do not eliminate the risk of occult disease [4, 5]. For patients with clinical T1N0 NSCLC, the prediction task is therefore used to estimate the residual risk of occult lymph node metastasis (oLNM) after clinical staging.

The consolidation-to-tumour ratio (CTR) on thin-section computed tomography (CT) reflects the proportion of the tumour occupied by the solid component and is associated with nodal involvement in early-stage NSCLC [6, 7]. Previous studies have reported a higher incidence of lymph node metastasis (LNM) and a more invasive phenotype in patients with tumours having CTR > 0.5 than in those with a CTR ≤ 0.5 [6]. However, the risk of LNM varies considerably even within the subgroup of patients with a CTR > 0.5 [8]. Combining preoperative information may therefore improve the estimation of residual oLNM risk in clinically node-negative patients with a CTR > 0.5.

In patients with NSCLC, pathological staging, prognostic assessment, and surgical planning are determined on the basis of lymph node status [9, 10]. A randomized

controlled trial revealed that sublobar resection was noninferior to lobectomy for disease-free survival in patients with peripheral NSCLC measuring ≤2 cm and a confirmed node-negative status after adequate lymph node assessment [11]. The JCOG0802 trial revealed superior overall survival with segmentectomy in patients with small peripheral NSCLC [12]. These findings support the individualised surgical management of early-stage NSCLC. Recent studies have proposed matching treatment intensity to individual tumour risk to avoid undertreatment in high-risk patients and unnecessary treatment burden in low-risk patients [13]. The accurate estimation of nodal metastatic risk may inform the treatment approach; underestimating the nodal risk in patients with oLNM may lead to pathological understaging, affecting subsequent treatment planning, whereas extensive nodal intervention may increase the surgical burden in low-risk patients, with limited additional benefit [14, 15]. The evidence supporting sublobar resection has been mainly derived from patients with tumours ≤2 cm. Evidence to guide nodal management remains limited for patients with clinical T1N0 NSCLC tumours measuring >2 to ≤3 cm and a CTR > 0.5. More accurate preoperative estimates of occult nodal involvement may help inform nodal assessment and surgical planning in this subgroup.

Machine-learning models can combine preoperative clinical information to estimate individual risk. Wu et al. developed a model for patients with tumours ≤2 cm, providing preliminary evidence of the model effectiveness for LNM risk stratification [16]. Many existing models, however, have been developed within restricted

tumour-size ranges, particularly tumours ≤2 cm, and geographically independent external validation has not been conducted for these models. Their applicability to other populations therefore remains uncertain. Complex models may also provide limited insights into how individual predictions are generated, which may hinder their use in preoperative nodal assessment [17]. SHapley Additive exPlanations (SHAP) quantifies each feature's contribution to a prediction, helping clinicians interpret the model output [18]. It provides an overall assessment of feature importance and explains feature contributions to individual predictions.

In this multicentre study, we developed and externally validated an interpretable machine-learning model to estimate the preoperative oLNM risk in patients with clinical T1N0 NSCLC, an overall tumour diameter ≤3 cm, and a CTR > 0.5. We assessed model performance and its potential clinical utility and used SHAP to examine feature contributions at the population and patient levels.

Methods

Data sources

This multicentre retrospective study included a development cohort of 1,784 patients who underwent thoracoscopic pulmonary resection at the Department of Thoracic Surgery of the Affiliated Hospital of Southwest Medical University between June 2023 and June 2026. An independent external validation cohort included 525 patients who underwent elective thoracoscopic pulmonary resection at the Department of Thoracic Surgery of the First Affiliated Hospital of Zhengzhou University between June 2025 and June 2026. The same inclusion and exclusion criteria were applied at

both centres. The patient selection process is shown in Figure 1.

This study was conducted in accordance with the Declaration of Helsinki and was approved by the Institutional Review Board of the Affiliated Hospital of Southwest Medical University and the relevant Ethics Committee of the First Affiliated Hospital of Zhengzhou University, with the approval numbers of KY2026415 and 2026KS215, respectively.

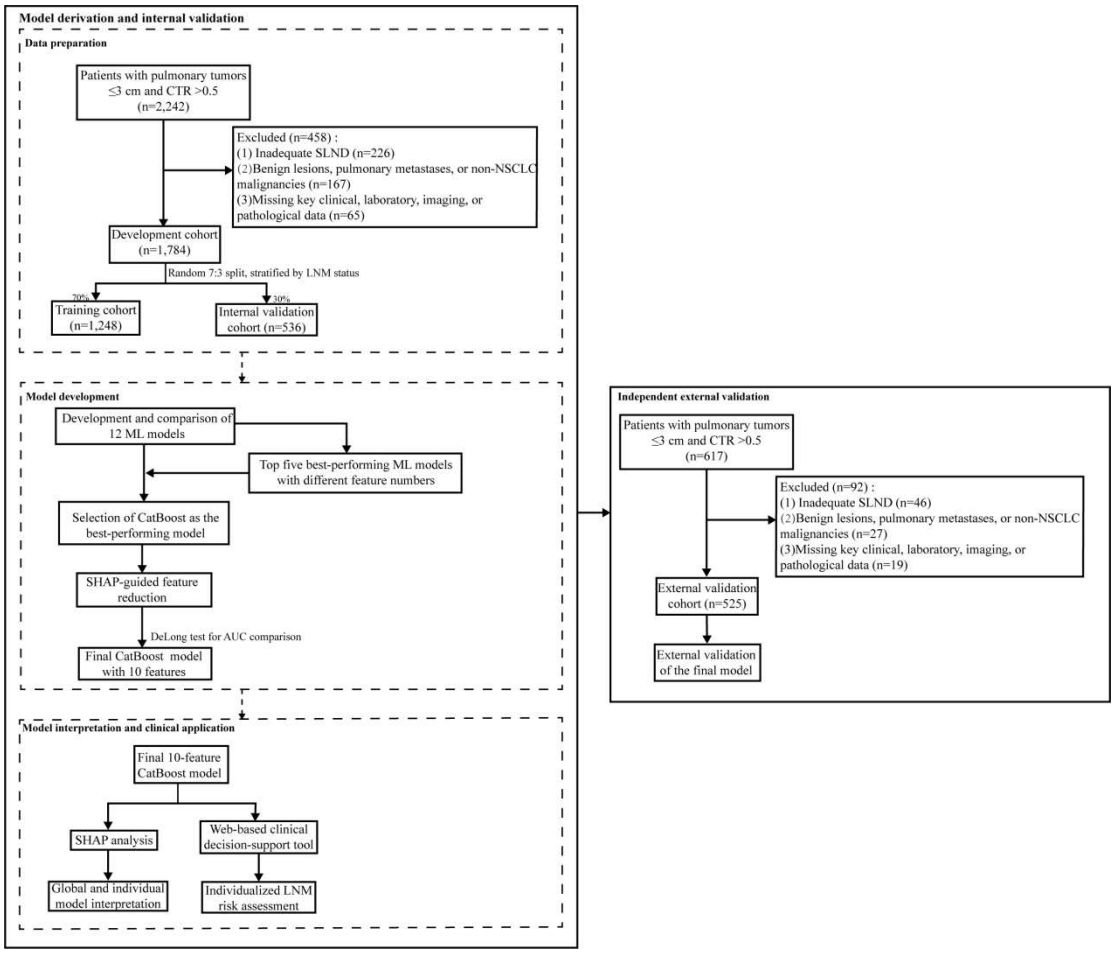


Fig. 1. Patient selection and study design.

AUC, area under the receiver operating characteristic curve; CTR, consolidation-to-tumor ratio; ML, machine learning; NSCLC, non-small cell lung cancer; oLNM, occult lymph node metastasis; SHAP, SHapley Additive exPlanations; SLND, systematic lymph node dissection.

Inclusion and exclusion criteria

The inclusion criteria were as follows: (1) clinical T1 disease based on preoperative assessment according to the ninth edition of the TNM classification; (2) clinical N0 (cN0) disease based on preoperative nodal assessment; (3) a maximum overall tumour diameter of ≤3 cm on preoperative chest CT; (4) a CTR > 0.5; (5) thoracoscopic pulmonary resection with systematic lymph node dissection (SLND); and (6) postoperative histopathological confirmation of NSCLC.

The exclusion criteria were as follows: (1) no surgical treatment or failure to undergo SLND to meet the study requirements; (2) postoperative pathological confirmation of a benign lesion, pulmonary metastasis, or other non-NSCLC pathologies; and (3) missing key clinical, laboratory, imaging, or pathological data.

Definitions and outcome assessment

Clinical N0 (cN0) was defined as the absence of regional lymph node metastasis on routine preoperative staging, based on chest CT and other staging examinations performed when clinically indicated.

CTR was defined as the ratio of the maximum diameter of the solid component to the maximum overall tumour diameter on preoperative thin-section chest CT. Pure-solid nodules were assigned a CTR of 1.0. Both measurements were performed on lung-window images.

Occult lymph node metastasis (oLNM) was defined as pathologically confirmed regional nodal metastasis (pN+) identified after resection in patients preoperatively classified as cN0.

SLND was performed according to the established standards for systematic lymph node evaluation and involved the complete removal of mediastinal lymph node–bearing tissue within defined anatomical boundaries. The dissection included at least three mediastinal lymph node stations, including Station 7, as well as the evaluation of hilar and intrapulmonary lymph nodes [19].

Feature collection and calculation

Preoperative demographic characteristics, vital signs, laboratory test results, and other clinical data were obtained from electronic medical records, and these data were considered candidate predictors. Laboratory measurements obtained within 7 days before surgery were used. To reduce the potential effects of multicollinearity on model stability and predictive performance, correlations among candidate features were assessed using Spearman rank correlation analysis. When two features were highly correlated (absolute Spearman correlation coefficient $|\rho| > 0.6$), the feature more strongly associated with the outcome was retained. After screening, 46 candidate features were retained for model development and validation (Supplementary Figure 1, Additional file 1).

Inflammation- and nutrition-related indices were calculated from preoperative complete blood counts and blood biochemical measurements. These indices included the modified systemic inflammation score (mSIS), neutrophil-to-platelet ratio (NPR), platelet-to-albumin ratio (PAR), prognostic nutritional index (PNI), neutrophil-to-lymphocyte ratio (NLR), aggregate index of systemic inflammation (AISI), systemic immune-inflammation index (SII), neutrophil-to-lymphocyte–

platelet ratio (NLPR), systemic inflammation response index (SIRI), lymphocyte-to-monocyte ratio (LMR), platelet-to-lymphocyte ratio (PLR), and neutrophil-to-monocyte ratio (NMR).

These indices were calculated as follows: NLR = N/L; PLR = P/L; NMR = N/M; LMR = L/M; SII = (N × P)/L; NLPR = N/(L × P); SIRI = (N × M)/L; AISI = (N × M × P)/L; NPR = N/P; PAR = P/ALB; and PNI = ALB + 5 × L. N, L, M, and P represent the absolute peripheral blood neutrophil, lymphocyte, monocyte, and platelet counts, respectively ($\times 10^9$/L), and ALB represents the serum albumin concentration (g/L).

The mSIS was determined from serum albumin concentration and LMR. A score of 0 was assigned when ALB was ≥40 g/L and LMR was ≥3.4; a score of 1 when only one value was below its respective threshold; and a score of 2 when ALB was <40 g/L and LMR was <3.4.

Model development and comparison

A total of 1,784 patients from the Affiliated Hospital of Southwest Medical University constituted the development cohort. Patients were stratified by oLNM status and randomly divided at a 7:3 ratio into a training cohort (n = 1,248) and an internal validation cohort (n = 536). All 46 candidate preoperative features were included in the initial model development.

Using the training cohort, we developed and compared 12 machine-learning algorithms: CatBoost, extreme gradient boosting (XGBoost), light gradient boosting machine (LightGBM), extremely randomized trees (ET), support vector machine (SVM), k-nearest neighbours (KNN), random forest (RF), artificial neural network

(ANN), gradient boosting machine (GBM), adaptive boosting (AdaBoost), logistic regression (LR), and decision tree (DT). These algorithms estimated the probability of oLNM in the study population. Hyperparameters were determined using Bayesian optimisation combined with manual fine-tuning. All model training and hyperparameter optimisation processes were performed exclusively on the training data; the internal validation data were not used for model fitting or hyperparameter selection.

The candidate models were compared using the internal validation cohort to select the algorithm for feature reduction and final model development. Fivefold and tenfold cross-validation were also performed to assess the stability of the model performance.

Feature selection and model interpretation

We used SHAP to quantify each feature's contribution to the model predictions and ranked the features by their mean absolute SHAP values. Features were progressively removed from the lowest to the highest importance, and the model was rebuilt after each step. AUCs for different feature sets were compared using the DeLong test, and features were removed until a statistically significant decrease in discrimination was observed. Among the models without a statistically significant reduction in AUC, predictive performance and parsimony were jointly considered to select the final 10-feature CatBoost model.

SHAP was used to interpret the final model at the global and individual levels. Global interpretation assessed the relative magnitude and direction of feature contributions to model predictions. Individual interpretation quantified each feature's

contribution to the model output for a given patient.

External validation

The independent cohort of 525 patients from the First Affiliated Hospital of Zhengzhou University was used for geographic external validation of the model. The final model architecture, input features, and parameter settings remained unchanged, with no retraining or optimisation using the external data. The model was applied directly to this cohort to assess its discrimination, calibration, and potential clinical utility, and generalizability across centres. An exploratory subgroup analysis evaluated model performance in patients with an overall tumour diameter of >2 to ≤3 cm.

Web-based prediction tools

The final model was deployed as an interactive web application using Streamlit. After the required preoperative features are entered, the application provides the predicted probability of oLNM and generates a SHAP force plot showing each feature's contribution to the individual prediction in real time.

Statistical analysis

All statistical analyses and model development procedures were performed using Python version 3.9.5 and R version 4.1.0. Continuous variables are summarized as the mean ± standard deviation or median (interquartile range), as appropriate, and the variables were compared using the independent-samples *t*-test or Mann–Whitney U test. Categorical variables are presented as frequencies and percentages, and the variables were compared using the χ^2 test or Fisher's exact test, as appropriate.

Discrimination was assessed using receiver operating characteristic (ROC) curves and the area under the curve (AUC), along with 95% confidence intervals (CIs). Predicted probabilities were converted into binary classifications using the CatBoost model's default probability threshold of 0.5. Sensitivity, specificity, positive predictive value, negative predictive value, accuracy, and F1 score were calculated from these classifications. Model calibration was conducted using calibration curves, and the overall predictive accuracy was assessed using the Brier score. The model's potential clinical utility was evaluated through decision curve analysis. The AUCs were compared using the DeLong test, where appropriate. All statistical tests were two-sided, and $P < 0.05$ was considered to indicate statistical significance.

Results

Patient characteristics

This study included 2,309 patients with clinical T1N0 NSCLC, an overall tumour diameter ≤3 cm, and a CTR > 0.5 from two centres. The development cohort included 1,784 patients, of whom 295 (16.5%) had oLNM (Table 1). In the independent external validation cohort, 97 of 525 patients (18.5%) had oLNM (Supplementary Table 1, Additional file 1). The difference in oLNM prevalence between the cohorts was not statistically significant ($P = 0.330$; Supplementary Table 2). Patient selection and the study design are provided in detail in Figure 1.

In the development cohort, compared with patients without oLNM, those with oLNM were more often male and more frequently had a smoking history (both $P <$

0.001). Compared with patients without oLNM, patients with oLNM had a higher NLR and a lower LMR (both $P < 0.001$), as well as higher levels of carcinoembryonic antigen (CEA), cancer antigen 125 (CA125), and cytokeratin 19 fragment 21-1 (CYFRA21-1) (all $P < 0.001$).Their tumors were larger, had higher CTR values, and were more often nonperipheral ($P < 0.001$, $P < 0.001$, and $P = 0.007$, respectively). Histological type also differed between patients with and without oLNM ($P = 0.003$; Table 1).

Table 1. Development cohort characteristics according to occult lymph node metastasis status.

Variables	without oLNM(n=1489)	oLNM(n=295)	P value
Sex			<0.001
Male	558 (37.5%)	159 (53.9%)	
Female	931 (62.5%)	136 (46.1%)	
Age, year	57.40±10.78	59.19±9.41	0.047
Weight, kg	60.63±10.75	61.87±10.30	0.068
Height, m	1.61±0.08	1.62±0.08	0.011
BMI, kg/m^2	23.24±3.21	23.37±3.05	0.528
Smoking			<0.001
no	1195 (80.3%)	202 (68.5%)	
yes	294 (19.7%)	93 (31.5%)	
Drinking			0.187
no	1290 (86.6%)	247 (83.7%)	
yes	199 (13.4%)	48 (16.3%)	
Lung disease			0.280
no	1389 (93.3%)	270 (91.5%)	
yes	100 (6.7%)	25 (8.5%)	
Diabetes			0.576
no	1353 (90.9%)	265 (89.8%)	
yes	136 (9.1%)	30 (10.2%)	
Hypertension			0.724

Variables	without oLNM(n=1489)	oLNM(n=295)	P value
no	1070 (71.9%)	209 (70.8%)	
yes	419 (28.1%)	86 (29.2%)	
CAD			0.791
no	1366 (91.7%)	272 (92.2%)	
yes	123 (8.3%)	23 (7.8%)	
Cerebral infarction			0.658
no	1403 (94.2%)	276 (93.6%)	
yes	86 (5.8%)	19 (6.4%)	
K, mmol/L	4.14 [3.89–4.38]	4.15 [3.92–4.44]	0.164
Na, mmol/L	142.50 [141.00–144.00]	143.00 [141.00–144.00]	0.917
Cl, mmol/L	105.00 [103.00–106.90]	105.00 [103.00–106.00]	0.049
ALT, U/L	15.00 [11.00–21.00]	16.00 [11.00–24.00]	0.158
AST, U/L	18.00 [15.00–21.00]	18.00 [15.00–22.00]	0.168
PT, seconds	10.70 [10.20–11.20]	10.40 [9.80–10.90]	<0.001
APTT, seconds	28.80 [26.90–31.00]	29.30 [27.10–31.00]	0.312
TT, seconds	16.10 [14.80–18.00]	15.80 [14.50–17.60]	0.020
Fbg, g/L	2.72 [2.39–3.12]	2.80 [2.44–3.29]	0.025
D-dimer, mg/L	0.18 [0.07–0.25]	0.19 [0.07–0.27]	0.760
WBC, 10^9/L	5.54 [4.68–6.62]	5.70 [4.86–6.78]	0.074
RBC, 10^{12}/L	4.34 [4.04–4.62]	4.33 [4.07–4.63]	0.976
Hb, g/L	133.00 [123.00–142.00]	134.00 [125.00–144.00]	0.106
PLT, 10^9/L	219.00 [184.00–259.00]	216.00 [187.00–248.00]	0.431
NEU%	57.80 [52.60–63.40]	58.40 [52.75–64.30]	0.317
NEU, 10^9/L	3.18 [2.56–4.06]	3.27 [2.69–4.13]	0.090
LYM, 10^9/L	1.78 [1.45–2.22]	1.78 [1.50–2.14]	0.883
MO, 10^9/L	0.36 [0.29–0.45]	0.38 [0.30–0.47]	0.024
Hct, L/L	0.40 [0.37–0.43]	0.40 [0.37–0.42]	0.980
ALB, g/L	42.90 [40.40–45.40]	42.00 [39.75–44.55]	0.439
mSIS			0.045
0	950 (63.8%)	179 (60.7%)	
1	451 (30.3%)	87 (29.5%)	
2	88 (5.9%)	29 (9.8%)	
NPR	0.01 [0.01–0.02]	0.02 [0.01–0.02]	0.005

Variables	without oLNM(n=1489)	oLNM(n=295)	P value
PAR	5.14 [4.29–6.06]	5.14 [4.21–5.93]	0.287
PNI	52.00 [48.90–55.20]	51.40 [48.38–54.30]	0.062
NLR	1.81 [1.35–2.45]	2.22 [1.74–3.06]	<0.001
AISI	143.48 [86.84–228.30]	147.89 [92.36–258.50]	0.216
SII	392.95 [274.70–561.49]	385.32 [271.60–585.19]	0.948
NLPR	0.01 [0.01–0.01]	0.01 [0.01–0.01]	0.009
SIRI	0.66 [0.44–1.00]	0.70 [0.48–1.14]	0.019
LMR	4.93 [3.69–6.39]	3.77 [2.49–5.22]	<0.001
PLR	121.78 [93.48–156.67]	124.07 [92.94–152.82]	0.639
NMR	8.85 [7.21–10.97]	8.57 [7.04–10.80]	0.219
AFP, ng/mL	3.07 [2.17–4.06]	3.53 [2.27–4.82]	<0.001
CEA, ng/mL	2.04 [1.20–3.32]	2.89 [1.75–4.89]	<0.001
CA125, U/mL	9.41 [6.64–13.30]	12.43 [9.75–18.45]	<0.001
CA19-9, U/mL	10.07 [5.89–15.40]	11.10 [6.83–17.14]	0.021
CA72-4, U/mL	2.61 [1.27–4.89]	2.73 [1.13–5.12]	0.878
CYFRA21-1, ng/mL	1.83 [1.12–2.80]	2.58 [1.81–3.84]	<0.001
NSE, ng/mL	11.50 [6.48–15.57]	12.80 [6.59–16.07]	0.210
Tumor size, cm	1.80 [1.10–2.50]	2.50 [1.90–2.70]	<0.001
Periphery			0.007
Peripheral	1431 (96.1%)	273 (92.5%)	
Non-peripheral	58 (3.9%)	22 (7.5%)	
Pathologic histology			0.003
Adenocarcinoma	1385 (93.0%)	261 (88.5%)	
Squamous cell carcinoma	62 (4.2%)	26 (8.8%)	
Other	42 (2.8%)	8 (2.7%)	
Tumor location			0.448
RUL	527 (35.4%)	103 (34.9%)	
RML	106 (7.1%)	27 (9.2%)	
RLL	236 (15.8%)	45 (15.3%)	
LUL	411 (27.6%)	71 (24.1%)	
LLL	209 (14.0%)	49 (16.6%)	
CTR	0.75 [0.63–0.87]	0.87 [0.76–0.95]	<0.001

Data are presented as mean ± SD for normally distributed continuous variables, median [interquartile range] for non-normally distributed continuous variables, and n (%) for categorical variables.

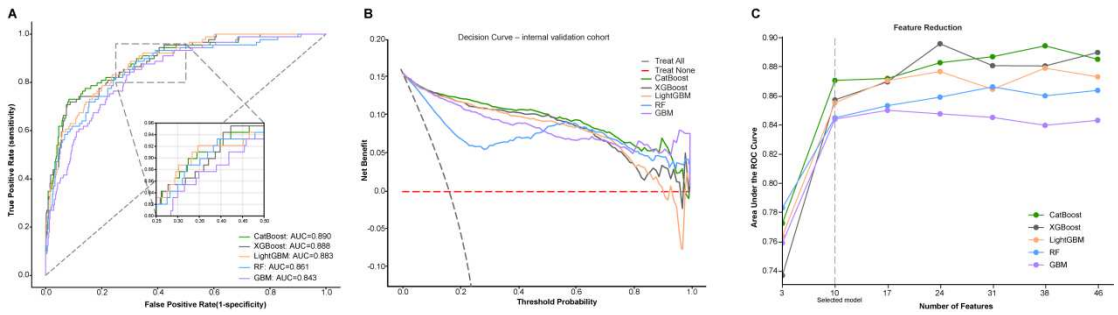
AFP, alpha-fetoprotein; AISI, aggregate index of systemic inflammation; ALB, albumin; ALT, alanine aminotransferase; APTT, activated partial thromboplastin time; AST, aspartate aminotransferase; BMI, body mass index; CA125, cancer antigen 125; CA19-9, carbohydrate antigen 19-9; CA72-4, carbohydrate antigen 72-4; CAD, coronary artery disease; CEA, carcinoembryonic antigen; CTR, consolidation-to-tumor ratio; CYFRA21-1, cytokeratin 19 fragment 21-1; Fbg, fibrinogen; Hct, hematocrit; Hb, hemoglobin; LLL, left lower lobe; LMR, lymphocyte-to-monocyte ratio; LUL, left upper lobe; LYM, lymphocyte count; MO, monocyte count; mSIS, modified systemic inflammation score; NLR, neutrophil-to-lymphocyte ratio; NLPR, neutrophil-to-lymphocyte–platelet ratio; NMR, neutrophil-to-monocyte ratio; NPR, neutrophil-to-platelet ratio; NSE, neuron-specific enolase; oLNM, occult lymph node metastasis; PAR, platelet-to-albumin ratio; PLR, platelet-to-lymphocyte ratio; PNI, prognostic nutritional index; PT, prothrombin time; RBC, red blood cell count; RLL, right lower lobe; RML, right middle lobe; RUL, right upper lobe; SD, standard deviation; SII, systemic immune-inflammation index; SIRI, systemic inflammation response index; TT, thrombin time; WBC, white blood cell count.

Similar findings were observed in the external validation cohort. Patients with oLNM had a higher NLR, a lower LMR (both $P < 0.001$), and higher CEA, CA125, and CYFRA21-1 levels than those without oLNM did ($P = 0.001$, $P < 0.001$, and $P < 0.001$, respectively). Their tumours were larger and had higher CTR values (both $P < 0.001$), and nonperipheral lesions were more frequent ($P < 0.001$). Histological type also differed between the groups ($P = 0.031$). Smoking history and previous

pulmonary disease were more common in patients with oLNM (P = 0.022 and P = 0.002, respectively), whereas sex did not significantly differ between the groups (P = 0.726; Supplementary Table 1).

Model development and performance comparison

We developed and compared 12 machine-learning models using 46 preoperative features. In the internal validation cohort, the highest AUC was determined for CatBoost (0.890; 95% CI, 0.851–0.928), followed by the AUCs for XGBoost (0.888; 95% CI, 0.853–0.922) and LightGBM (0.883; 95% CI, 0.846–0.916). The AUCs for the remaining models ranged from 0.704 to 0.861. Performance metrics for all 12 models are presented in Supplementary Figure 2 and Supplementary Table 3. The ROC curves and decision curves for the five best-performing models are presented in Figures 2A and 2B. The SHAP summary plots of the top 20 features for each model are provided in Supplementary Figures 3A–E. Given its highest AUC value and the balanced predictive performance, CatBoost was selected for feature reduction and model interpretation (Figure 2C).



298

299 **Fig. 2. Performance comparison and feature reduction of machine-learning models.**

300 (A) Receiver operating characteristic (ROC) curves for the five models with the highest observed
301 AUCs in the internal validation cohort. (B) Decision curves for the same five models across threshold
302 probabilities. (C) AUCs of these models with varying numbers of features.

303 AUC, area under the receiver operating characteristic curve; DCA, decision curve analysis; GBM,
304 gradient boosting machine; LightGBM, light gradient boosting machine; RF, random forest; ROC,
305 receiver operating characteristic; XGBoost, extreme gradient boosting.

306 **Feature reduction and final model selection**

307 We evaluated the CatBoost models with progressively fewer features on the basis
308 of the feature importance rankings. The AUC varied moderately across a range of
309 feature counts (Supplementary Figures 4B and 4C). The 46-feature model had an
310 AUC of 0.890. The 10-feature model had an AUC of 0.870, which did not differ
311 significantly from that of the full model (ΔAUC = 0.020; P = 0.090). Reducing the
312 feature count to nine features decreased the AUC to 0.854, which was significantly
313 different from that of the full model (ΔAUC = 0.036; P = 0.009). With a reduction to
314 three features, the AUC decreased to 0.772 (ΔAUC = 0.118, P < 0.001;
315 Supplementary Figure 4A). Performance metrics for the different feature sets are
316 provided in Supplementary Table 4.

On the basis of discrimination, model complexity, and clinical feasibility, we selected a 10-feature CatBoost model comprising tumour size, CTR, CYFRA21-1, CA125, LMR, PLR, prothrombin time (PT), monocyte count (MO), NLR, and neuron-specific enolase (NSE). In the internal validation cohort, this model had an AUC of 0.870 (95% CI, 0.827–0.906). At the default probability threshold of 0.5, the sensitivity, specificity, positive predictive value, negative predictive value, accuracy, and F1 score were 0.618, 0.913, 0.585, 0.923, 0.864, and 0.601, respectively.

In supplementary analyses of internal stability, the final model had a mean AUC of 0.905 ± 0.020 with fivefold cross-validation and 0.885 ± 0.038 with tenfold cross-validation (Supplementary Figure 5A and 5B), suggesting its relatively stable discrimination across data partitions.

Comparison of the final model with individual predictors

In the internal validation cohort, the final CatBoost model had a greater AUC (0.870) than that of any individual predictor (Supplementary Figure 6A). NLR had the highest individual AUC (0.693), followed by CYFRA21-1 (0.690), CA125 (0.677), LMR (0.675), CTR (0.665), and tumour size (0.656). Differences in AUCs between the final model and individual predictors ranged from 0.177 to 0.353 and were statistically significant according to the DeLong test (all $P < 0.001$).

Decision curve analysis revealed greater net benefit for the final CatBoost model than for any individual predictor across a broad range of threshold probabilities (Supplementary Figure 6B).

External validation of the final model

In the independent external validation cohort, the final 10-feature CatBoost model had an AUC of 0.855 (95% CI, 0.814–0.895; Figure 3A). The AUC did not differ significantly from that in the internal validation cohort (ΔAUC = 0.015; 95% CI, −0.054 to 0.085; P = 0.657). The same fixed probability threshold of 0.5 was applied to the external validation cohort. The resulting sensitivity, specificity, positive predictive value, and negative predictive value were 0.588, 0.895, 0.559, and 0.905, respectively.

The Brier score in the external validation cohort was 0.112. The calibration curve showed generally close agreement between the predicted probabilities of oLNM risk and the observed oLNM rates in the lower-risk range, with some overestimation of the risk at intermediate-to-high predicted probabilities (Figure 3B). Decision curve analysis revealed that the final model provided greater net benefit than the treat-all and treat-none strategies across a broad range of threshold probabilities (Figure 3C).

An exploratory subgroup analysis was performed in 296 patients with an overall tumour diameter >2 to ≤3 cm, of whom 68 (23.0%) had oLNM. The model achieved an AUC of 0.852 (95% CI, 0.802–0.898; Figure 3D), with accuracy, sensitivity, specificity, positive predictive value, and negative predictive value of 0.787, 0.647, 0.829, 0.530, and 0.887, respectively. The Brier score was 0.136. Calibration showed some disagreement between the predicted and observed risks at intermediate-to-high predicted probabilities (Figure 3E). Decision curve analysis revealed greater net benefit for the final model than the treat-all and treat-none strategies over parts of the

low-to-intermediate threshold probability range (Figure 3F).

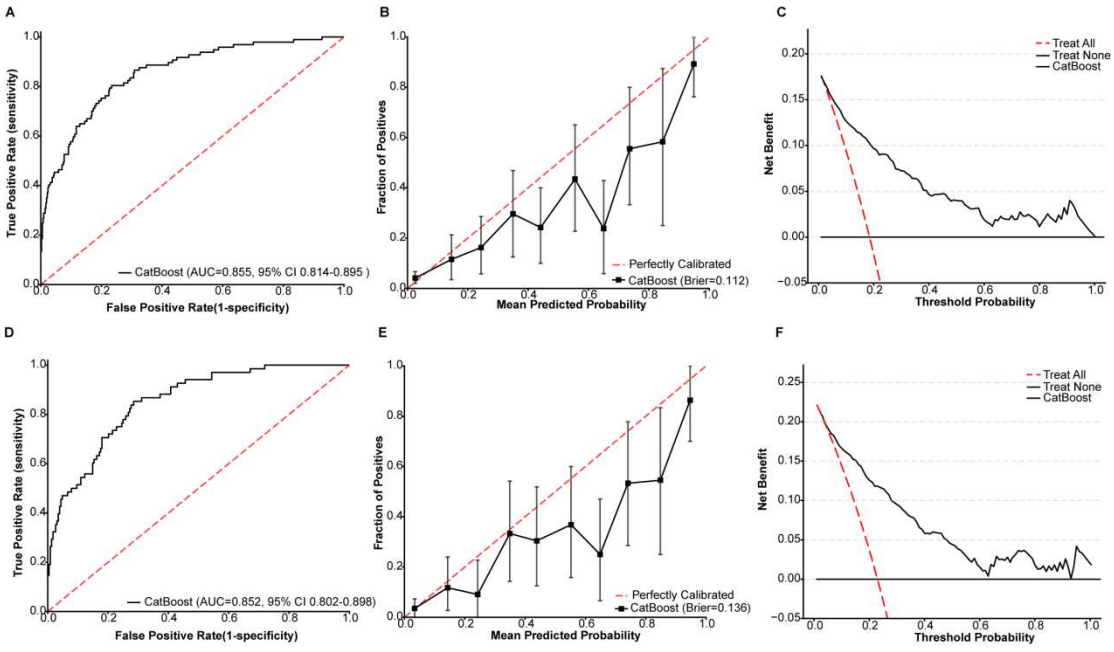


Fig. 3. External validation and exploratory subgroup analysis of the final 10-feature CatBoost model.

(A–C) Performance in the overall external validation cohort (n=525): (A) receiver operating characteristic curve, (B) calibration curve, and (C) decision curve. (D–F) Performance in the external validation subgroup with an overall tumor diameter >2 to ≤3 cm (n=296): (D) receiver operating characteristic curve, (E) calibration curve, and (F) decision curve.

AUC, area under the receiver operating characteristic curve; CI, confidence interval; oLNM, occult lymph node metastasis.

Model interpretation

We used SHAP to examine feature contributions to the final 10-feature CatBoost model at the global and individual levels. On the basis of feature ranking by mean absolute SHAP value, tumour size contributed the most to the model predictions,

followed by CTR, CYFRA21-1, CA125, LMR, PLR, PT, MO, NLR, and NSE (Figure 4A). The summary plot shows how feature values are related to the direction of their contributions (Figure 4B). Larger tumours and higher CTR, CYFRA21-1, CA125, and NLR generally shifted predictions towards oLNM, whereas higher LMR, PLR, PT, and MO generally shifted predictions in the opposite direction. These relationships were not uniformly linear. In the dependence plots, the SHAP values for tumour size and CTR generally changed from negative to positive as their values increased, whereas a higher LMR generally contributed to a lower predicted oLNM risk (Figure 4C). Pronounced nonlinear patterns were noted for PLR, PT, MO, and NSE, with their contributions varying across the observed feature values.

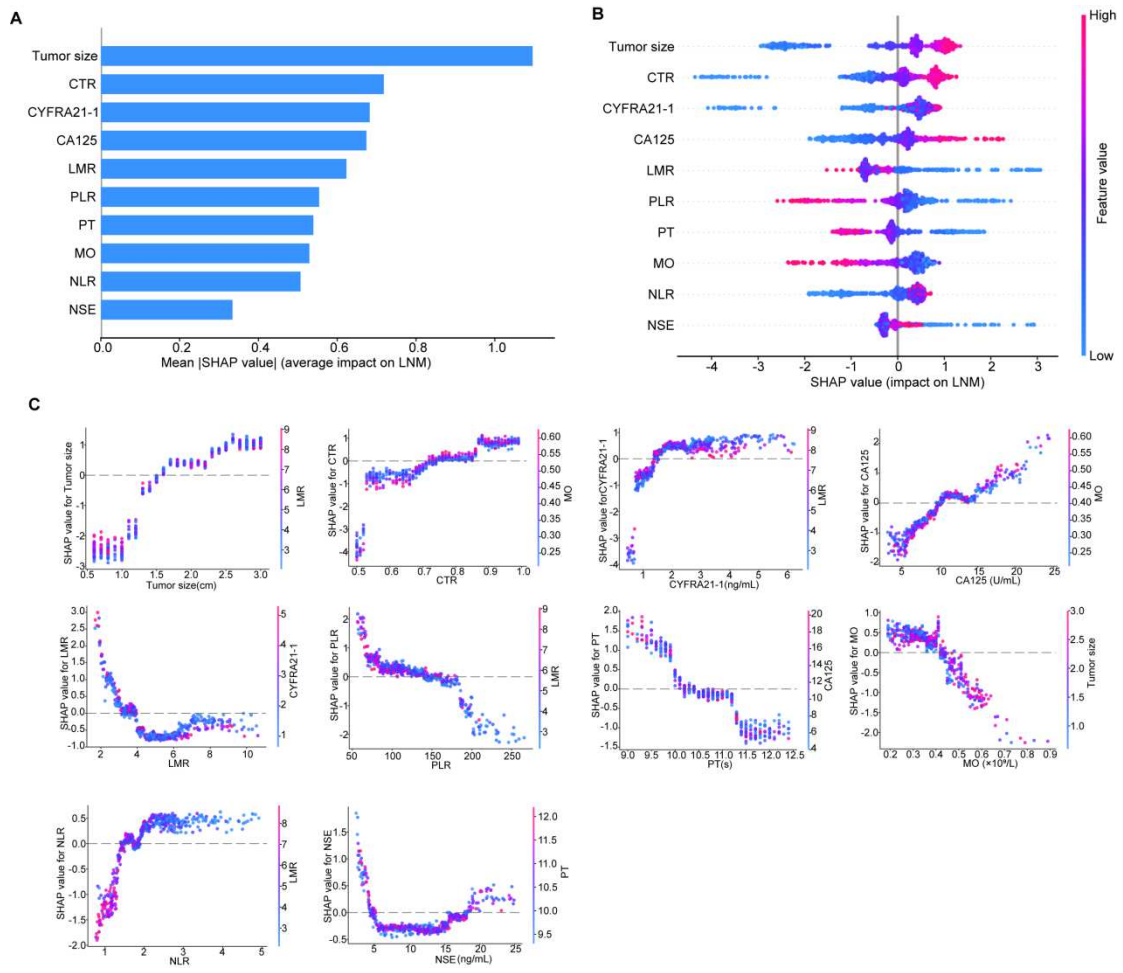


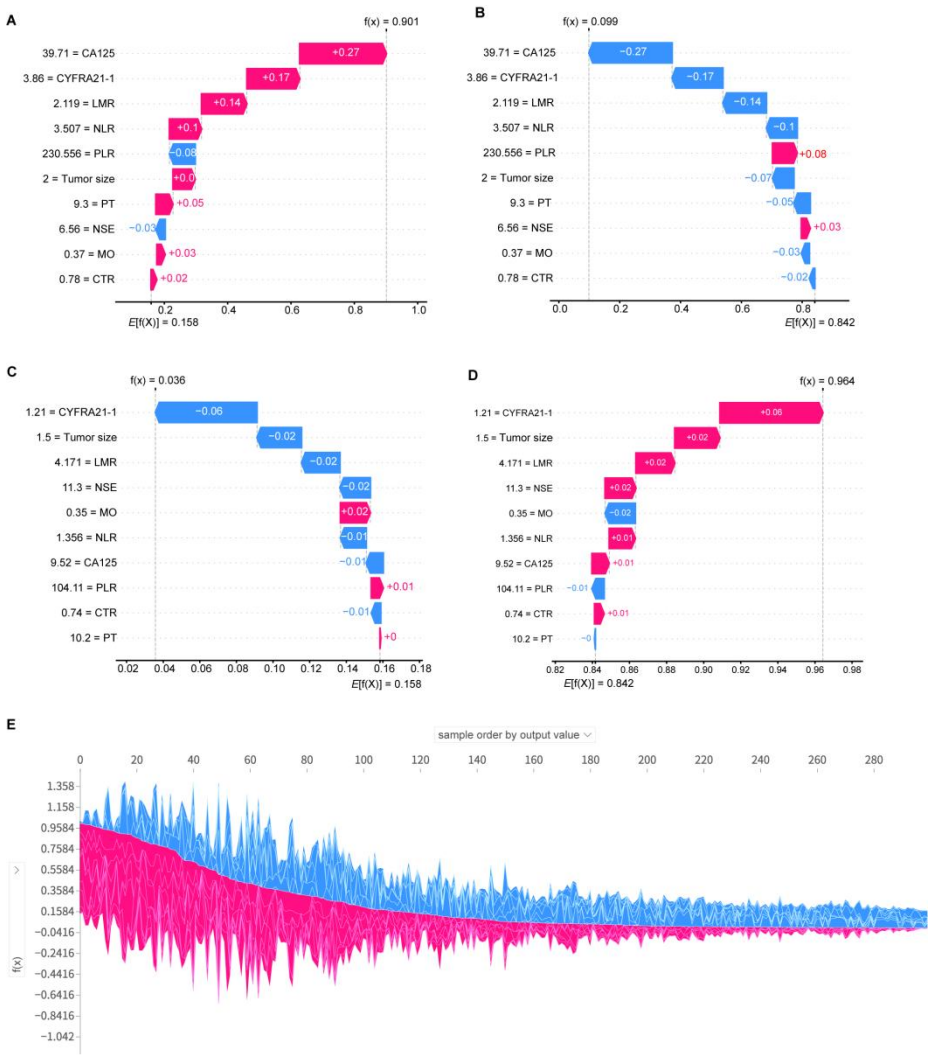
Fig. 4. SHAP-based interpretation of the final 10-feature CatBoost model.

(A) Global feature importance ranking based on mean absolute SHAP values. (B) SHAP summary plot showing the impact of feature values on oLNM predictions. (C) SHAP dependence plots illustrating the nonlinear relationships between selected features and model output.

CTR, consolidation-to-tumor ratio; CYFRA21-1, cytokeratin 19 fragment 21-1; LMR, lymphocyte-to-monocyte ratio; MO, monocyte count; NLR, neutrophil-to-lymphocyte ratio; NSE, neuron-specific enolase; PLR, platelet-to-lymphocyte ratio; PT, prothrombin time; SHAP, SHapley Additive exPlanations.

SHAP waterfall plots illustrate the predictions for individual patients (Figures 5A–D). For a patient with pathologically confirmed oLNM, the predicted oLNM

probability was 90.1% (Figure 5A). CA125 (39.71 U/mL), CYFRA21-1 (3.86 ng/mL), LMR (2.119), and NLR (3.507) were the main contributors to oLNM, with the greatest contributions from CA125 and CYFRA21-1. PLR (230.556) and NSE (6.56 ng/mL) shifted the prediction away from oLNM. The complementary prediction for the same patient is shown in Figure 5B, with a 9.9% probability of no oLNM. For a patient without oLNM, the predicted oLNM probability was 3.6% (Figure 5C). Lower CYFRA21-1 levels (1.21 ng/mL), smaller tumour size (1.5 cm), and LMR (4.171) were the main contributors to a lower predicted risk. The corresponding probability of no oLNM was 96.4% (Figure 5D). The SHAP decision plot shows the cumulative feature contributions and their variation among patients in the internal validation cohort (Figure 5E).



406

407 **Fig. 5. Patient-level SHAP interpretation of the final 10-feature CatBoost model.**

408 (A, B) SHAP waterfall plots for a patient with pathologically confirmed oLNM, showing predicted
409 probabilities of 90.1% for oLNM and 9.9% for no oLNM, respectively. (C, D) Corresponding plots for
410 a patient without oLNM, showing predicted probabilities of 3.6% for oLNM and 96.4% for no oLNM,
411 respectively. (E) SHAP decision plot showing cumulative feature contributions across patients in the
412 internal validation cohort.

413 oLNM, occult lymph node metastasis; SHAP, SHapley Additive exPlanations.

414 ## Web-based prediction tools

415 The final 10-feature CatBoost model was deployed as an interactive web-based tool

for the individualised estimation of oLNM risk (Figure 6). After the 10 features are entered, the tool provides the predicted probability of oLNM and generates a SHAP force plot showing each feature's contribution to the individual prediction in real time. The tool is available at https://lnminclinicalt1lungcancer.streamlit.app/.

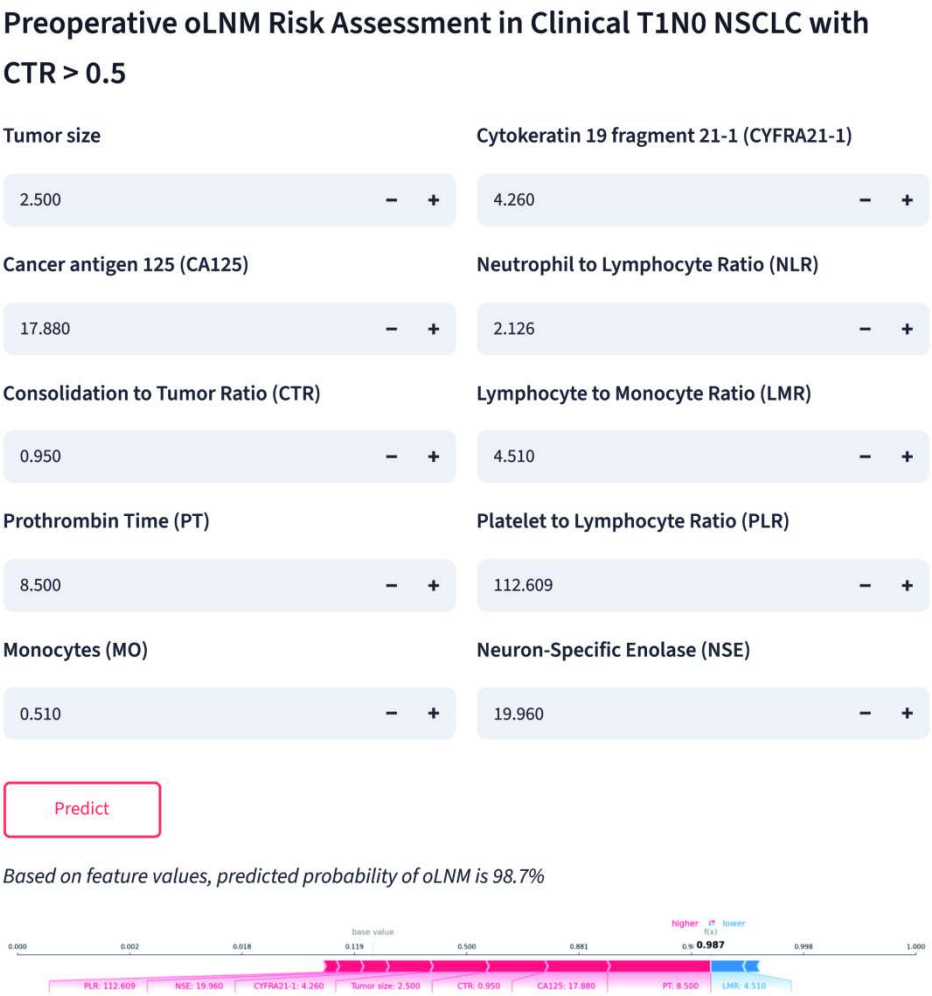


Fig. 6. Web-based application of the final 10-feature CatBoost model for oLNM risk assessment.

After entry of the 10 required features, the application displays the predicted probability of oLNM and a SHAP force plot. In the example shown, the predicted probability of oLNM is 98.7%. Red features increase the prediction for oLNM, whereas blue features decrease it.

oLNM, occult lymph node metastasis; SHAP, SHapley Additive exPlanations.

Discussion

Patients with clinical T1N0 NSCLC may develop nodal metastases that remain undetected until pathological examination [20, 21]. In this study, oLNM was identified in 16.5% of patients in the development cohort and 18.5% in the external validation cohort, indicating residual nodal risk despite a cN0 classification. These rates may partly reflect the restriction to patients with a CTR > 0.5, a radiological phenotype associated with greater invasiveness, and the use of SLND in all patients, which enabled comprehensive pathological nodal assessment. Conventional preoperative imaging has limited sensitivity for the microscopic examination of nodal disease and occult N1/N2 metastases [4]. Thus, cN0 status alone cannot reliably exclude pathological nodal involvement. Additional preoperative risk stratification may help identify patients with a higher probability of residual oLNM and supplement established nodal staging and pathological assessment.

Previous studies have predicted nodal metastasis in early-stage NSCLC using clinical characteristics, conventional imaging, PET/CT-derived parameters, radiomics, and multivariable models [22-25]. Radiomics and deep-learning approaches, however, often require image segmentation, complex feature extraction, and standardization across platforms, which may hinder their reproducibility and routine implementation [26, 27]. Our final CatBoost model used 10 routinely available preoperative variables reflecting the tumour burden, radiological invasiveness, tumour markers, systemic inflammation and immunity, and coagulation function. It required no specialized

448 image postprocessing or additional testing platforms. SHAP-guided feature selection
449 reduced the feature set from 46 to 10, with a moderate decrease in the observed AUC.
450 The model showed good discrimination in cross-validation and independent external
451 validation. Decision curve analysis revealed greater net benefit for the final model
452 than for individual predictors over a range of threshold probabilities. These findings
453 support the potential use of routinely collected measurements for estimating oLNM
454 risk.

455 Tumour size contributed the most to the prediction, which is consistent with
456 previous studies associating larger tumours with more aggressive behaviour and nodal
457 metastasis in early-stage NSCLC [28, 29]. CTR ranked second in terms of feature
458 contributions, which is consistent with the previous associations found among a
459 greater solid component, tumour invasiveness, and nodal involvement [12, 30, 31].
460 CYFRA21-1, CA125, and NSE were also retained in the model; these variables have
461 been linked to the tumour burden and nodal metastasis [32-36]. NLR, LMR, PLR, and
462 monocyte count reflect systemic inflammatory and immune responses that are
463 implicated in tumour progression and lymphatic metastasis [37-40]. The contribution
464 of PT suggests that coagulation-related measurements may also provide information
465 relevant to nodal metastatic risk [41, 42]. Although individual predictors had limited
466 discrimination, the model combining 10 features exhibited better performance. These
467 findings are consistent with the multifactorial nature of oLNM risk and support
468 combining complementary clinical and biological information for estimating nodal
469 metastatic risk.

A predicted probability alone does not explain how a model arrives at its estimate, which can make the result difficult to assess clinically [43]. SHAP was used to quantify feature contributions to the CatBoost model at both the population and patient levels [44]. Globally, tumour size, CTR, CYFRA21-1, CA125, and inflammation-related variables were the major contributors to the prediction. For individual patients, SHAP showed how specific feature values shifted the model output towards or away from oLNM risk. These explanations may help clinicians interpret risk estimates, alongside conventional clinical findings, and the web application presents them in an accessible format. However, SHAP values describe contributions within the fitted model. They do not establish causal effects or demonstrate that changing a variable would alter a patient's oLNM risk [45].

Recent work on early-stage NSCLC has advocated tailoring treatment intensity to individual tumour risk and anatomical stage to avoid undertreatment and unnecessary intervention [13]. Residual oLNM risk is one component of this assessment in patients classified as cN0. In patients with clinical T1N0 NSCLC, overall tumour diameter ≤3 cm, and CTR > 0.5, our model may provide additional risk stratification alongside conventional nodal staging. A higher predicted risk may help identify patients who warrant particular attention during nodal assessment, whereas lower risk estimates may help identify patients with a lower predicted probability of occult disease. Nevertheless, model predictions alone should not determine the extent of lymph node dissection or justify reducing or omitting SLND. Any change in nodal management based on these predictions requires prospective validation and formal

evaluation of clinical impact.

This study has several limitations. Its retrospective design remains susceptible to selection bias, information bias, and residual confounding despite the relatively large cohort and independent external validation. In addition, preoperative nodal staging was conducted according to routine clinical practice without a uniform imaging or invasive staging protocol. Differences in the staging work-up may have affected cN0 classification and the observed prevalence of oLNM. The external validation of the model was conducted in patients from only one independent centre. Therefore, model performance should be further assessed across institutions, geographical regions, and clinical settings. Potentially informative data, including PET/CT metabolic parameters, radiomic features, and molecular alterations, were not incorporated into the model. Although these data may provide additional biological information, the model's reliance on a small set of routinely available preoperative variables may facilitate clinical implementation. Finally, the model was developed to estimate oLNM risk in this study; however, its use for direct nodal management has not been established. The optimal clinical thresholds and the utility of the model for preoperative mediastinal staging, intraoperative nodal assessment, and patient outcomes remain uncertain. Prospective multicentre validation and clinical impact studies are needed, along with an assessment of whether selected multimodal data improve predictive performance beyond routine preoperative variables.

Conclusions

In this study, we developed and externally validated an interpretable model to

estimate preoperative oLNM risk in patients with clinical T1N0 NSCLC, an overall tumour diameter ≤3 cm, and a CTR > 0.5. The 10-feature CatBoost model showed good discrimination, as demonstrated by internal and external validation. SHAP was used to quantify feature contributions to individual predictions. The model may supplement conventional nodal staging by improving the accuracy of preoperative risk assessment. The prospective validation of the model is required to determine its clinical impact and role in guiding nodal management.

List of abbreviations

AISI, aggregate index of systemic inflammation; ALB, albumin; ANN, artificial neural network; AUC, area under the receiver operating characteristic curve; CA125, cancer antigen 125; CEA, carcinoembryonic antigen; CI, confidence interval; cN0, clinical node-negative status; CT, computed tomography; CTR, consolidation-to-tumour ratio; CYFRA21-1, cytokeratin 19 fragment 21-1; DCA, decision curve analysis; DT, decision tree; ET, extremely randomized trees; GBM, gradient boosting machine; KNN, k-nearest neighbours; LightGBM, light gradient boosting machine; LMR, lymphocyte-to-monocyte ratio; LNM, lymph node metastasis; LR, logistic regression; MO, monocyte count; mSIS, modified systemic inflammation score; NLR, neutrophil-to-lymphocyte ratio; NLPR, neutrophil-to-lymphocyte–platelet ratio; NMR, neutrophil-to-monocyte ratio; NPR, neutrophil-to-platelet ratio; NSCLC, non-small cell lung cancer; NSE, neuron-specific enolase; oLNM, occult lymph node metastasis; PAR, platelet-to-albumin ratio; PET/CT, positron emission tomography/computed tomography; PLR, platelet-to-lymphocyte ratio; PNI, prognostic nutritional index; PT, prothrombin time; RF, random forest; ROC, receiver operating characteristic; SHAP, SHapley

Additive exPlanations; SII, systemic immune-inflammation index; SIRI, systemic inflammation response index; SLND, systematic lymph node dissection; SVM, support vector machine; TNM, tumour–node–metastasis; XGBoost, extreme gradient boosting.

Declarations

Ethics approval and consent to participate

This study was conducted in accordance with the Declaration of Helsinki and approved by the Institutional Review Board of the Affiliated Hospital of Southwest Medical University (approval No. KY2026415) and the Ethics Committee of the First Affiliated Hospital of Zhengzhou University (approval No. 2026KS215). The requirement for informed consent was waived by both ethics committees owing to the retrospective nature of the study.

Consent for publication

Not applicable.

Availability of data and materials

The datasets used and/or analysed during the current study are available from the corresponding author on reasonable request.

Competing interests

The authors declare that they have no competing interests.

Funding

This study was supported by a university-level research grant from Southwest Medical University (grant number 2025JC121).

Authors' contributions

Yanmin Zhou designed and conducted the study, analysed the data, and wrote the first draft.

Dengguo Zhang, Zhengpan Wei, Jiangtao Pu, and Biao Wang contributed to study design and data collection. Zhulin Wang and Xiangnan Li conceived the project. All authors read and approved the final manuscript.

Acknowledgements

Not applicable.

Additional files

Additional file 1. Supplementary tables and figures. File format: DOCX. Supplementary Tables 1–4 and Supplementary Figures 1–6 present cohort characteristics, model performance, correlation analysis, feature selection, cross-validation, and comparisons with individual predictors.

References

1. Hung JJ, Yeh YC, Jeng WJ, Wu YC, Chou TY, Hsu WH: **Factors predicting occult lymph node metastasis in completely resected lung adenocarcinoma of 3 cm or smaller**. *Eur J Cardiothorac Surg* 2016, **50**(2):329-336.

2. Huang X, Huang X, Wang K, Liu L, Jin G: **Predictors of occult lymph node metastasis in clinical T1 lung adenocarcinoma: a retrospective dual-center study**. *BMC Pulm Med* 2025, **25**(1):99.

3. Huang J, Osarogiagbon RU, Giroux DJ, Nishimura KK, Bille A, Cardillo G, Detterbeck F, Kernstine K, Kim HK, Lievens Y *et al*: **The International Association for the Study of Lung Cancer Staging Project for Lung Cancer: Proposals for the Revision of the N Descriptors in the Forthcoming Ninth Edition of the TNM Classification for Lung Cancer**. *J Thorac Oncol* 2024, **19**(5):766-785.

4. Silvestri GA, Gonzalez AV, Jantz MA, Margolis ML, Gould MK, Tanoue LT, Harris LJ, Detterbeck

FC: **Methods for staging non-small cell lung cancer: Diagnosis and management of lung cancer, 3rd ed: American College of Chest Physicians evidence-based clinical practice guidelines**. *Chest* 2013, **143**(5 Suppl):e211S-e250S.

5. De Leyn P, Dooms C, Kuzdzal J, Lardinois D, Passlick B, Rami-Porta R, Turna A, Van Schil P, Venuta F, Waller D *et al*: **Revised ESTS guidelines for preoperative mediastinal lymph node staging for non-small-cell lung cancer**. *Eur J Cardiothorac Surg* 2014, **45**(5):787-798.

6. Sun X, Xin Y, Jia Y, Wang H, Cui X, Chen J: **Mediastinal lymph node metastasis pattern of subsolid non-small cell lung cancer**. *J Thorac Dis* 2026, **18**(6):655.

7. Chen YC, Lin YH, Chien HC, Hsu PK, Hung JJ, Huang CS, Hsieh CC, Hsu WH, Hsu HS: **Preoperative consolidation-to-tumor ratio is effective in the prediction of lymph node metastasis in patients with pulmonary ground-glass component nodules**. *Thorac Cancer* 2021, **12**(8):1203-1209.

8. Li D, Li S, Zhang H, Xia C, Nan X, Liu H, Chen J: **Development and validation of a predictive model for lymph node metastases in peripheral non-small cell lung cancer with a tumor diameter ≤ 2.0 cm and a consolidation-to-tumor ratio > 0.5**. *Front Oncol* 2025, **15**:1436771.

9. Detterbeck FC, Boffa DJ, Kim AW, Tanoue LT: **The Eighth Edition Lung Cancer Stage Classification**. *Chest* 2017, **151**(1):193-203.

10. Rami-Porta R, Nishimura KK, Giroux DJ, Detterbeck F, Cardillo G, Edwards JG, Fong KM, Giuliani M, Huang J, Kernstine KH, Sr. *et al*: **The International Association for the Study of Lung Cancer Lung Cancer Staging Project: Proposals for Revision of the TNM Stage Groups in the Forthcoming (Ninth) Edition of the TNM Classification for Lung Cancer**. *J Thorac Oncol* 2024, **19**(7):1007-1027.

11. Altorki N, Wang X, Kozono D, Watt C, Landrenau R, Wigle D, Port J, Jones DR, Conti M, Ashrafi AS *et al*: **Lobar or Sublobar Resection for Peripheral Stage IA Non-Small-Cell Lung Cancer**. *N Engl J Med* 2023, **388**(6):489-498.

12. Saji H, Okada M, Tsuboi M, Nakajima R, Suzuki K, Aokage K, Aoki T, Okami J, Yoshino I, Ito H *et al*: **Segmentectomy versus lobectomy in small-sized peripheral non-small-cell lung cancer (JCOG0802/WJOG4607L): a multicentre, open-label, phase 3, randomised, controlled, non-inferiority trial**. *Lancet* 2022, **399**(10335):1607-1617.

13. Zhang C, Gu X, Wang P, Li D, Zhang G, Wang T, Wu P, Rao W, Muhammad S, Tan B *et al*: **Early stage nonsmall cell lung cancer: Toward a risk-adaptive paradigm in the era of biologic precision**. *CA Cancer J Clin* 2026, **76**(5):e70100.

14. Woo W, Shin JI, Kipkorir V, Yang YH, Lee S, Lee CY: **Clinical Benefits of Lobe-Specific Lymph Node Dissection in Surgery for NSCLC: A Systematic Review and Meta-Analysis**. *JTO Clin Res Rep* 2023, **4**(5):100516.

15. Darling GE, Allen MS, Decker PA, Ballman K, Malthaner RA, Inculet RI, Jones DR, McKenna RJ, Landreneau RJ, Rusch VW *et al*: **Randomized trial of mediastinal lymph node sampling versus complete lymphadenectomy during pulmonary resection in the patient with N0 or N1 (less than hilar) non-small cell carcinoma: results of the American College of Surgery Oncology Group Z0030 Trial**. *J Thorac Cardiovasc Surg* 2011, **141**(3):662-670.

16. Wu Y, Liu J, Han C, Liu X, Chong Y, Wang Z, Gong L, Zhang J, Gao X, Guo C *et al*: **Preoperative Prediction of Lymph Node Metastasis in Patients With Early-T-Stage Non-small Cell Lung Cancer by Machine Learning Algorithms**. *Front Oncol* 2020, **10**:743.

17. Reddy S: **Explainability and artificial intelligence in medicine**. *Lancet Digit Health* 2022,

4(4):e214-e215.

18. Van Dort BA, Engelsma T, Sneekes P, Peute L, Medlock S: **Explainable AI in hospital clinical decision support systems: A scoping review of healthcare professionals' perspectives**. *PLOS Digit Health* 2026, **5**(5):e0001417.

19. Lardinois D, De Leyn P, Van Schil P, Porta RR, Waller D, Passlick B, Zielinski M, Lerut T, Weder W: **ESTS guidelines for intraoperative lymph node staging in non-small cell lung cancer**. *Eur J Cardiothorac Surg* 2006, **30**(5):787-792.

20. Lee PC, Port JL, Korst RJ, Liss Y, Meherally DN, Altorki NK: **Risk factors for occult mediastinal metastases in clinical stage I non-small cell lung cancer**. *Ann Thorac Surg* 2007, **84**(1):177-181.

21. Kawamoto N, Mimae T, Tsutani Y, Kamigaichi A, Tsubokawa N, Miyata Y, Okada M: **Tumor distance from the mediastinum predicts N2 upstaging in clinical stage I lower-lobe non-small cell lung cancer**. *J Thorac Cardiovasc Surg* 2024, **167**(2):488-497.e482.

22. Tang Y, Garu A, Chen X, Guan Z, Cai X, Huang H, Xitao L, Tang K, Dong Y: **Risk factors for mediastinal lymph node metastases in early-stage non-small-cell lung cancer and prediction model establishment**. *Am J Cancer Res* 2024, **14**(12):5952-5964.

23. Feng Y, Zhang H, Yu J, Wang L, Wu Y, Zhu L, Zheng J, Chen Y, Lai J, Yang H *et al*: **Preoperative Contrast-enhanced CT Features Associated with Occult Lymph Node Metastasis in Early-Stage Solid Non-Small Cell Lung Cancer**. *Radiol Imaging Cancer* 2026, **8**(2):e250448.

24. Ouyang ML, Xia HW, Xu MM, Lin J, Wang LL, Zheng XW, Tang K: **Prediction of occult lymph node metastasis using SUV, volumetric parameters and intratumoral heterogeneity of the primary tumor in T1-2N0M0 lung cancer patients staged by PET/CT**. *Ann Nucl Med* 2019,

33(9):671-680.

25. Yin X, Lu Y, Cui Y, Zhou Z, Wen J, Huang Z, Yan Y, Yu J, Meng X: **CT-based radiomics-deep learning model predicts occult lymph node metastasis in early-stage lung adenocarcinoma patients: A multicenter study**. *Chin J Cancer Res* 2025, **37**(1):12-27.

26. Li J, Wei J, Pan R, Ma D, Xie Z, Gao Z: **Multicenter peritumoral radiomics in oncology: advances, challenges, and future directions**. *Radiat Oncol* 2026, **21**(1).

27. Shao J, Wei M, Li K, Lv G, Liu K, Guo Y: **Radiomics: Current Applications and Future Directions**. *MedComm (2020)* 2026, **7**(6):e70773.

28. Chen B, Wang X, Yu X, Xia WJ, Zhao H, Li XF, Liu LX, Liu Y, Hu J, Fu XN *et al*: **Lymph node metastasis in Chinese patients with clinical T1 non-small cell lung cancer: A multicenter real-world observational study**. *Thorac Cancer* 2019, **10**(3):533-542.

29. Zhao JL, Guo HW, Yang P, Jiang DZ, Tian H: **Selective lymph node dissection for clinical T1 stage non-small cell lung cancer**. *Transl Cancer Res* 2019, **8**(8):2820-2828.

30. Zheng Y, Ju S, Huang R, Zhao J: **Lymph node metastasis risk factors in clinical stage IA3 lung adenocarcinoma**. *J Cancer Res Ther* 2023, **19**(1):34-38.

31. Fang C, Xiang Y, Han W: **Preoperative risk factors of lymph node metastasis in clinical N0 lung adenocarcinoma of 3 cm or less in diameter**. *BMC Surg* 2022, **22**(1):153.

32. Yu Z, Zhang G, Yang M, Zhang S, Zhao B, Shen G, Chai Y: **Systematic review of CYFRA 21-1 as a prognostic indicator and its predictive correlation with clinicopathological features in Non-small Cell Lung Cancer: A meta-analysis**. *Oncotarget* 2017, **8**(3):4043-4050.

33. Tang J, Shu HY, Sun T, Zhang LJ, Kang M, Ying P, Ling Q, Zou J, Liao XL, Wang YX *et al*: **Potential factors of cytokeratin fragment 21-1 and cancer embryonic antigen for mediastinal lymph**

node metastasis in lung cancer. *Front Genet* 2022, **13**:1009141.

34. Li JX, Feng GY, He KL, Li GS, Gao X, Yan GQ, Wei LQ, He X, Li Y, Fu ZW *et al*: **Preoperative prediction of occult lymph node metastasis in patients with non-small cell lung cancer: a simple and widely applicable model**. *BMC Pulm Med* 2024, **24**(1):557.

35. Wang J, Wang X, Mao Y, Niu H, Zhao F, Shen D, Wang L: **Peripheral blood tumor marker levels can indicate the location of lung cancer metastasis**. *Oncol Lett* 2025, **30**(6):545.

36. Li Q, Sang S: **Diagnostic Value and Clinical Significance of Combined Detection of Serum Markers CYFRA21-1, SCC Ag, NSE, CEA and ProGRP in Non-Small Cell Lung Carcinoma**. *Clin Lab* 2020, **66**(11).

37. Huang C, Yue J, Li Z, Li N, Zhao J, Qi D: **Usefulness of the neutrophil-to-lymphocyte ratio in predicting lymph node metastasis in patients with non-small cell lung cancer**. *Tumour Biol* 2015, **36**(10):7581-7589.

38. Chen W, Xu M, Sun Y, Ji C, Chen L, Liu S, Zhou K, Zhou Z: **Integrative Predictive Models of Computed Tomography Texture Parameters and Hematological Parameters for Lymph Node Metastasis in Lung Adenocarcinomas**. *J Comput Assist Tomogr* 2022, **46**(2):315-324.

39. Wei B, Jin X, Lu G, Zhao T, Xue H, Zhang Y: **A novel nomogram to predict lymph node metastasis in cT1 non-small-cell lung cancer based on PET/CT and peripheral blood cell parameters**. *BMC Pulm Med* 2023, **23**(1):44.

40. Jiang S, Zhao J, Feng J, Yu Y, Zhang L, Huang C, Zhang Z: **Integrative Single-Cell and Machine Learning Analysis Reveals Immune Microenvironment Remodelling in Lymph Node Metastasis of Lung Adenocarcinoma**. *J Cell Mol Med* 2025, **29**(18):e70859.

41. Bayleyegn B, Adane T, Getawa S, Aynalem M, Kifle ZD: **Coagulation parameters in lung cancer**

patients: A systematic review and meta-analysis. *J Clin Lab Anal* 2022, **36**(7):e24550.

42. Du C, Liu Q, Guo Y, Gong J, Yan L, Li Z, Niu C: **Prediction of Lung Cancer Metastasis Using Machine Learning Models Based on Clinical Laboratory Data**. *Cancer Rep (Hoboken)* 2025, **8**(10):e70350.

43. Rudin C: **Stop Explaining Black Box Machine Learning Models for High Stakes Decisions and Use Interpretable Models Instead**. *Nat Mach Intell* 2019, **1**(5):206-215.

44. Lundberg SM, Erion G, Chen H, DeGrave A, Prutkin JM, Nair B, Katz R, Himmelfarb J, Bansal N, Lee SI: **From Local Explanations to Global Understanding with Explainable AI for Trees**. *Nat Mach Intell* 2020, **2**(1):56-67.

45. Ghassemi M, Oakden-Rayner L, Beam AL: **The false hope of current approaches to explainable artificial intelligence in health care**. *Lancet Digit Health* 2021, **3**(11):e745-e750.

Supplementary Files

This is a list of supplementary files associated with this preprint. Click to download.

- Additionalfile.docx